Modeling of Concurrent CO_2 and Water Splitting by Practical Photoelectrochemical Devices

Ronald R. Gutierrez and Sophia Haussener*,z

Laboratory of Renewable Energy Science and Engineering, EPFL, 1015 Lausanne, Switzerland

Concurrent solar generation of hydrogen and CO through photoelectrochemical (PEC) water and CO_2 electrolysis, and the subsequent use of the product gas mixture in conventional Fischer-Tropsch processes, has the potential to provide a flexible pathway for direct solar generation of a variety of liquid fuels. In order for this approach to be practical, PEC devices must be designed to continuously and selectively provide a well-defined ratio of hydrogen to CO, independent of operating conditions. We develop a computational PEC device model providing insight into the dynamics and design requirements of such a device. We investigate a variety of combinations of catalysts (Ag, Cu, Ni, Pt, Co) and photoabsorbers (Si and Ga-based) under steady and transient solar irradiation conditions. Typical H_2/CO ratios of 0.1 were observed for Ag-based electrodes, and ratios of 5 when using Cu-based electrodes. Variation in catalyst and photoabsorber properties provided guidance for the development of catalysts allowing for a H_2/CO product ratio close to 2. Device design variations and the addition of Ni as a second cathode-side catalyst improved the generation of hydrogen, allowing H_2/CO ratios to reach between 1.7 and 2.15. Transient simulations showed that product ratios vary significantly over the day and year, implying the use of storage or controlling measures or the addition of a water gas shift reactor. Our model provides insights and practical considerations for the design and implementation of a PEC device for the concurrent production of hydrogen and CO.
 [DOI: 10.1149/2.0661610jes]

Manuscript submitted May 13, 2016; revised manuscript received July 25, 2016. Published August 25, 2016.

Solar liquid fuel production can potentially be achieved by the reduction of water and CO_2 through two non-biological pathways:[1–4] *i*) solar thermochemical (STC) approaches, and *ii*) photoelectrochemical (PEC) approaches. In both cases, water and CO_2 is split into hydrogen and CO (a mixture called synthesis gas) and, for PEC approaches only, other lower order hydrocarbon products. Synthesis gas can subsequently be used in a Fischer-Tropsch process to produce liquid fuels such as gasoline and diesel. In STC approaches, redox couples are used and alternatingly reduced then oxidized at temperatures above 1000 K while splitting water and CO_2. Synthesis gas is very selectively produced at a tailorable hydrogen to CO ratio.[5] In PEC approaches, water electrolysis has been achieved,[6] and the reduction of CO_2 has been demonstrated,[7–10] but with challenges in respect to product selectivity and efficiency. While the PEC production of CO requires the involvement of two electrons only, methanol or higher order hydrocarbon products require the involvement of six, eight, or even twelve electrons (Eqs. 5 and 6), presenting significant challenges for the development of efficient and selective catalysts. Assuming that STC and PEC approaches can be complementary solar fuel processing pathways, synthesis gas appears to be the obvious fuel choice, as it can be produced by both pathways (comparatively easy in the case of PEC compared to other products) and would subsequently require the same infrastructure for further processing and distribution. Furthermore, CO has been identified as the most cost-competitive electrochemically generated CO_2-reduction fuel.[11]

The low selectivity and operating condition-dependent product composition of PEC-based CO_2 reduction makes it challenging to predict the product composition and its variation with respect to the choice of the device components (i.e. photoabsorber, catalysts, electrolytes), device design (affecting overpotentials[12]), and variation in the operating conditions, such as daily and seasonal variation in irradiation.[13] Significantly higher overpotentials have been reported for CO_2 reduction compared to water splitting, requiring the use of photoabsorbers able to provide potentials above 2 V.

The characterization of the electrochemical reduction of CO_2 indicates that catalysts made of copper, silver, gold, zinc, palladium, and gallium provide activity and selectivity toward the production of CO.[14,8] Copper is among the few candidates which is not extremely rare,[15] but exhibits synthesis activity of other products, such as methane and ethylene. This activity has been shown to depend largely on catalyst morphology and synthesis routes.[16–19] Kuhl et al.[16] investigated the products of electrochemical CO_2 reduction in a solution of 0.1 M of $KHCO_3$ on a copper foil utilizing a custom-made electrochemical cell. Detailed insight into the product combination and its potential dependence was provided, and 16 different CO_2 products were identified. The maximum generation of methanol achieved was 0.124 μmol/cm^2/h, corresponding to a faradaic efficiency (FE) of 0.14% at −1.15 V vs RHE. Higher FEs were achieved for hydrogen, carbon monoxide, methane, formate, and ethylene. Le et at.[17] reduced CO_2 to methanol in 0.5 M potassium bicarbonate ($KHCO_3$) utilizing different copper oxides, namely air-oxidized copper, anodized copper, and cuprous oxide thin film electrodes. The results suggested that CH_3OH production may be associated with Cu(I) surface species which appeared to be reduced as CH_3OH was produced. The results also showed that Cu(I) sites promoted catalytic activity and selectivity. From the three electrodes studied, the highest performing was the cuprous oxide film, since Cu(I) sites were less reduced. Methanol yields of 43 μmol/cm^2/h and FE of 38% were observed at −1.32 V vs SHE.

Electrochemical CO_2 reduction with rare catalysts, such as silver in pH-neutral solutions, have shown that the main products are carbon monoxide and hydrogen,[20–22] and only minor products like formate, methane, methanol, and ethanol are observed.[23] Thorson et al.[24] investigated the CO_2 reduction by silver spray-painted gas diffusion layers in 16 different types of alkaline solutions, reporting that an improvement in the production of CO is achieved when large cations are present in the electrolyte. Silver supported on titania,[25] and carbon supported, nitrogen-based organometallic silver catalyst,[26] were characterized in alkaline solutions for the reduction of CO_2 resulting in the production of CO and H_2 only.

Barton et al.[7] reduced CO_2 to methanol using a p-GaP semiconductor immersed in 0.1 M acetate buffer containing 10 mM pyridine maintained at pH 5.2. Yields of 3.83 μmol/cm^2/h and 1.51 μmol/cm^2/h at potentials of −0.70 and −0.30 V vs SCE were achieved, corresponding to FEs of 56% and 90% respectively.

Still, all of the investigated catalysts provide selectivity toward the production of hydrogen. Consequently, the production of synthesis gas can potentially be achieved in a single PEC device, reducing the cost of synthesis gas production, which otherwise uses separated individual hydrogen and CO production devices and double auxiliary system components. However, it is unclear what a combined device would look like in terms of design, and how the component choices and operating conditions would affect the product combination. For example, design is expected to affect the overpotential of the device,[12,13] and

*Electrochemical Society Member.
zE-mail: sophia.haussener@epfl.ch

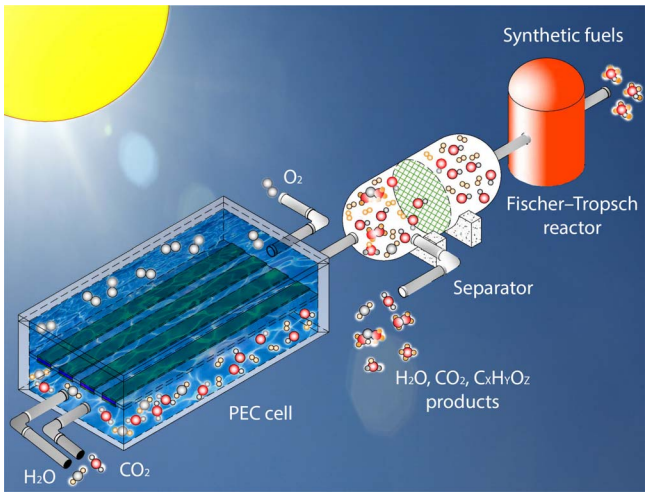

Figure 1. Schematic representation of the solar fuel synthesis process, consisting of a PEC device unit, a separator unit, and a Fischer-Tropsch reactor unit.

consequently affect product composition. In this example, could the same components be used with only the design changed to manage product composition? If one aims at the production of synthesis gas with a specific ratio of hydrogen to CO (for example: the production of methanol requires a ratio of 2), how should the design look and how can such a ratio be produced in a stable way over the year?

These are questions which we aim to address within the modeling framework developed and introduced in this work. We then use our model to providing guidelines for a practical PEC device concurrently producing hydrogen and CO. We start from designing a PEC device utilizing catalysts and photoabsorbers currently available. Design choices for enhanced efficiency and product selectivity are discussed and materials-related bottlenecks identified. Guidelines for the development of catalyst and photoabsorber characteristics are provided, giving specific product combinations and particular robustness toward variations in the operating conditions.

Governing Equations and Methodology

System description.—The complete system (Figure 1) consists of a PEC device, separator unit, and reactor. Water and carbon dioxide are fed to the PEC device where they are photoelectrochemically converted into a mixture of hydrogen, carbon monoxide, and other hydrocarbon products. The products of the PEC device pass through a separator unit in order to separate the desired synthesis gas from other products and the unconverted water and CO_2. The synthesis gas is then fed into a FT reactor where it is converted into liquid hydrocarbons.

The PEC device design considered here uses buried multi-junction photovoltaics (PV) decorated with catalysts.[27] The physical processes taking place in the PEC device consist of photon absorption, charge generation, charge transport, and charge separation in the photovoltaic cell. Holes are used at the anode for the oxygen evolution reaction, while electrons are used at the cathode for water and CO_2 reduction. Ions are transported in the electrolyte to ensure charge conservation.

A hydrogen to carbon monoxide ratio of approximately 2 is desired in a FT reactor if the production of liquid fuels is targeted. Exact ratios depend on the catalysts and operating conditions of the FT processes. For example, Co-based catalysts need a H_2/CO ratio of about 2.15 while Fe-based catalysts require ratios of about 1.7. The lower ratio of the latter is explained by a favored concurrent water-gas shift reaction.[28]

Model domain.—The modelling framework developed focuses on the PEC device only, one component of a complete system shown in Figure 1. The monolithic PEC device is modelled as a buried tandem PV cell covered by transparent conducting oxide (TCO) layer and catalyst layers on either side (or without the TCO layer).[27,4] The photoabsorber-catalyst sandwich is immersed in a liquid electrolyte and attached to a semi-permeable membrane ensuring efficient product separation while permitting the conduction of OH^- or $HCO3^-$ ions. A schematic of the modelled 2D unit cell in two different configurations is shown in Figure 2. Due to symmetry, half of the unit cell is modelled in order to reduce computational expense. The developed model follows the water-splitting PEC device model presented in.[12,13]

The reference dimensions used for all simulations were: an electrode length, l_{el}, of 1 cm, electrode thickness, t_{el}, of 10 μm, electrolyte height, h_{el}, of 1 cm, membrane length, l_{mem}, of 0.1 mm, and membrane thickness, t_{mem}, of 10 μm. Detailed investigations of the influence of dimensional choices on the performance are given in Ref. 12 We observed the same trends for our concurrent water and CO_2 electrolysis PEC device. One option of the sandwich and side-by-side PEC device designs uses a cathode composed of two catalysts, as shown in Figure 2. This two-catalyst cathode design is characterized by the dimensions of the individual catalyst patches, l_A and l_B, and the number of catalyst patches, n_A and n_B. The area fraction covered by both catalysts is then given by $(n_A l_A + n_B l_B)/(l_{el}/2)$. The order of the cathode catalysts can be varied, i.e. catalyst A is closest to the membrane and followed by catalyst B, or vice versa.

Assumptions.—Solar irradiation is intermittent and varies according to location and season. We assumed a constant irradiation of 1000 W/m^2 in the first part of this work in order to provide a straight-forward comparison of the different device designs and material combinations. In the second part of our study, transient simulations were conducted

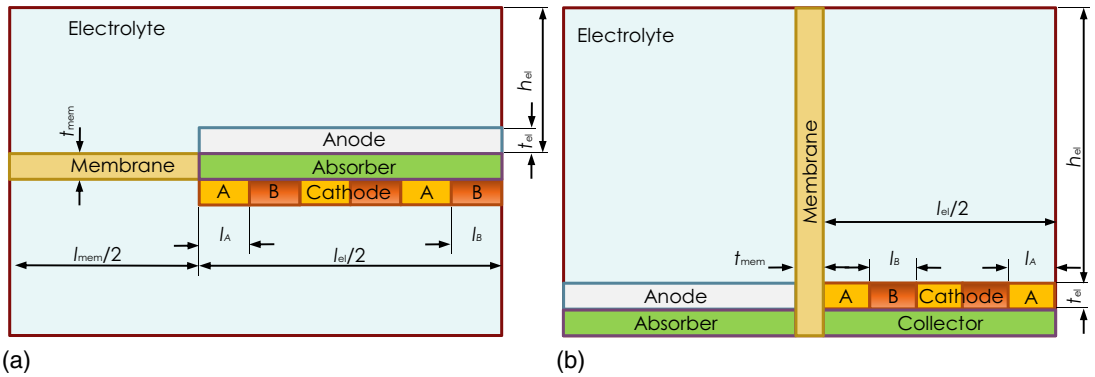

Figure 2. Unit cells of the two investigated PEC device designs, consisting of a photoabsorber, anode and cathode (the latter possibly incorporating two uniformly distributed catalysts), semi-permeable membrane, and electrolyte. The design in a) uses a sandwiched architecture, and the design in b) uses a side-by-side architecture.

using the irradiation data of Barstow, CA (USA), provided by NREL's TMY3 datasets. We assumed the AM1.5 spectrum and scaled it according to the irradiation magnitude.

Standard operational conditions for temperature and pressure were also assumed ($T = 20^{\circ}$C and $p = 1$ atm). More realistic simulations would take into account the increase in the system's temperature leading to a decrease in PV cell performance while also decreasing the required overpotentials for electrochemical reactions. We expect that smart thermal management can achieve a balance between these two competing effects.[13,29–31]

We assumed that the PEC device housing, the electrolyte, and the electrodes were radiatively non-participating in the spectral range relevant for the photoabsorber. Detailed investigation of the influence of the spectral absorption characteristics of the electrolyte on the performance can be found elsewhere.[32] An estimation of the thickness and absorption properties of the catalysts allowed for this assumption to be valid is discussed in the supporting information. Similarly, we neglected the light scattering by the generated bubbles. The bubbles were assumed not to disturb the system, which includes the assumption that no bubbles blocked the catalytically active area or changed the effective electrolyte conductivity.

We assumed that the electrolyte was well stirred and with a uniform concentration throughout the reactor. This assumption is valid for systems at the start of their operational time. This assumption allows the use of the simplified Nernst-Plank equation in the electrolyte domain.[35] Further assuming a quiescent electrolyte, the convection related ion transport can also be neglected, leading to migration related ion transport only and the validity of ohm's law. This assumption might be problematic for the investigated near-neutral system here, where the supporting electrolyte concentration develops significant gradients, introducing additional losses in the electrolysis part of the device eventually leading to device failure. Hernandez et al.[33] detail the time after which such a buffered system builds up significant gradients and potential losses. This time depends on the volume of the PEC device as well as the solution type and concentration. Modestino et al.[34] experimentally showed that engineering approaches can be introduced which actively counteract the buildup of the gradients and significantly extend the operational time of the device.

We assumed that CO_2 was constantly provided at a flow rate of 20 sccm, which, according to Kuhl et al.,[16] ensures sufficient CO_2 transport to the surface of the electrode while preventing interference from gas bubbles striking the surface. This assumption was verified by computing the stoichiometric CO_2 consumption at the surface resulting in about 8 sccm of CO_2, which is lower (by a factor two) compared to the inlet flow rate of CO_2, and therefore assures that CO_2 will not be depleted.

In all our simulations, the conductivity of the membrane was kept constant and equal to the conductivity of wet Nafion at room temperature. This simplification was acceptable because the membrane thickness was small compared to the ionic path through the electrolyte and the membrane characteristics were insignificant for our design and dimensional choices.[12,36] For the alkaline cases, an anion exchange membrane needs to be used.

Governing equations.—A typical diode-type correlation was used to model the current-voltage behavior of the tandem photovoltaics,

$$i_{PV} = i_l - i_d \exp\left(\frac{q\,(V + i_{PV}R_s)}{zkT}\right) - \frac{V + i_{PV}R_s}{R_{sh}}. \quad [1]$$

Two sets of PV cell types were modeled: *i*) realistically performing cells with optoelectric characteristics based on experimental measurements,[37–39] and *ii*) ideally performing cells with optoelectric characteristics based on the Shockley-Queisser limit.[40] The optoelectric characteristics of interest are: the light generated current, i_l, approximated by the short circuit current density, i_{sc}, the dark saturation current, i_d, the ideality factor, z, and the series and shunt resistances, R_s and R_{sh}.

We solved Ohm's law in the electrolyte, membrane, and electrode domains. For the boundary conditions, we assumed insulation at the electrolyte outer boundaries, a grounded cathode ($\phi_s = 0$ V), a voltage-dependent current input from the PV component (i_{op}) at the PV-electrode interfaces, and current continuity at the electrolyte-separator interface. The electrocatalytic reactions were modelled as a thin layer at the electrolyte-electrode interface using Butler-Volmer correlations,

$$i_{loc} = i_{loc,BV} = i_0\left(\exp\left(\frac{(1-\alpha)nF\eta}{RT}\right) - \exp\left(\frac{-\alpha nF\eta}{RT}\right)\right), \quad [2]$$

with exchange current densities, i_0, and charge transfer coefficients, α, experimentally measured for different catalysts and electrolytes.[41,42,24,16,43] In some cases an extended version of Eq. 2 was used,

$$i_{loc} = i_{loc,m} = \frac{i_{loc,BV}\cdot i_{lim}}{i_{lim} + |i_{loc,BV}|}, \quad [3]$$

to ensure a better fit to the experimental data. The limiting current density, i_{lim}, is estimated based on measured data for different catalysts and electrolytes.[41,42,24,16,43] Faraday's law was used to calculate the molar flux of the produced species. The operating current density, i_{op}, was obtained by simultaneously fulfilling Eqs. 1 to 3. The corresponding solar-to-fuel device efficiency was computed based on: the operational current density, the thermodynamic potential required to drive the reactions, U_θ, and the solar irradiation, I,

$$\eta_{PEC} = \frac{i_{op}U_\theta}{I}, \quad [4]$$

where for consistency U_θ was considered constant at 1.33 V, the larger potential difference of the reactions generating the two desired products (H_2 and CO).

Components choice.—*Electrocatalysts.*—We used silver and copper as catalysts for the CO_2 reduction. Multiple products have been observed when using these catalysts in different electrolytes. For silver in an alkaline solution, the major products are hydrogen and carbon monoxide.[24–26] The one-step reactions we considered at the cathode in alkaline solutions were:

$$CO_2 + H_2O + 2e^- \rightarrow CO + 2OH^-, \quad E^o = -0.932\,V \quad [5a]$$

$$2H_2O + 2e^- \rightarrow H_2 + 2OH^-, \quad E^o = -0.828\,V \quad [5b]$$

For copper and silver in a neutral solution, the production of formate, methane, methanol, ethylene, ethanol, and other minor products have been observed.[16,23] The one-step reactions we considered at the cathode in neutral solutions were:

$$3CO_2 + H_2O + 2e^- \rightarrow CO + 2HCO_3^-, \quad E^o = -0.567\,V \quad [6a]$$

$$2CO_2 + H_2O + 2e^- \rightarrow H_2 + 2HCO_3^-, \quad E^o = -0.463\,V \quad [6b]$$

$$2CO_2 + H_2O + 2e^- \rightarrow HCOO^- + HCO_3^-, \quad E^o = -0.688\,V \quad [6c]$$

$$9CO_2 + 6H_2O + 8e^- \rightarrow CH_4 + 8HCO_3^-, \quad E^o = -0.293\,V \quad [6d]$$

$$14CO_2 + 8H_2O + 12e^- \rightarrow C_2H_4 + 12HCO_3^-, \quad E^o = -0.384\,V \quad [6e]$$

$$14CO_2 + 9H_2O + 12e^- \rightarrow C_2H_6O + 12HCO_3^-, \quad E^o = -0.373\,V \quad [6f]$$

We used platinum as a counter electrode in alkaline and neutral solutions. Alternatively, cobalt oxide was used in an alkaline solution.

Table I. Electrocatalytic characteristics extracted from the different reported measurements in alkaline (1M KOH and 1 M NaOH) and neutral (0.1 M $KHCO_3$) solutions: exchange current density, i_0, charge transfer coefficient, α, and the limiting current density, i_{lim}. The corresponding Tafel slope, the valid overpotential range, and the goodness of the fit are also shown.

Electrode material	Supporting electrolyte	Product	i_0 (mA/cm^2)	Tafel slope (mV/dec)	α (-)	i_{lim} (mA/cm^2)	Overpotential range (V)	R^2 (-)
Silver	NaOH	Carbon monoxide	0.390	−226.4	0.128	72.24	−0.75 to −0.22	0.9993
		Hydrogen	0.014	−212.1	0.137	7.229	−0.85 to −0.32	0.9953
Silver	KOH	Carbon monoxide	0.466	−209	0.139	102.6	−0.59 to −0.22	0.9995
		Hydrogen	0.027	−254.7	0.114	5.234	−0.69 to −0.33	0.9593
Copper	$KHCO_3$	Carbon monoxide (1)	41.17	+181.6	0.160	-	−0.60 to −0.45	0.9286
		Carbon monoxide (2)	0.039	−783.6	0.037	-	−0.45 to 0	0.8893
		Hydrogen (1)	7.17e-6	−116.3	0.249	-	−0.7 to −0.6	0.9823
		Hydrogen (2)	0.052	−431.3	0.067	-	−0.6 to 0	0.9207
		Formate (1)	359.6	+123.5	0.235	0.419	−0.48 to −0.27	0.7555
		Formate (2)	0.013	−78.8	0.368	0.321	−0.27 to 0	0.9231
		Methane	5.46e-5	−171.4	0.042	-	−0.88 to 0	0.993
		Ethylene (1)	11.87	+915	0.005	-	−0.79 to −0.71	0.743
		Ethylene (2)	1.69e-4	−173	0.028	-	−0.71 to 0	0.9682
		Ethanol (1)	2320	+210.5	0.023	-	−0.79 to −0.72	0.8196
		Ethanol (2)	9.30e-6	−144.6	0.033	-	−0.72 to 0	0.9785
Nickel	NaOH	Hydrogen	8.31e-3	−141.1	0.206	-	−0.61 to −0.13	0.997
Platinum ox.	KOH	Oxygen	4.47e-6	+95	0.842	150	0.23 to 0.69	0.9985
Cobalt oxide	NaOH	Oxygen	1.23e-7	+53.9	0.726	-	0.23 to 0.44	0.9968
Platinum	$KHCO_3$	Oxygen (1)	0.594	+380.8	0.962	-	0 to 0.19	0.9946
		Oxygen (2)	0.197	+186.7	0.922	37.82	0.19 to 0.4	0.9953

The anodic reactions we considered for alkaline and neutral solutions, respectively, were:

$$4OH^- + 4h^+ \rightarrow O_2 + 2H_2O, \quad E^o = +0.401\,V \qquad [7a]$$

$$4HCO_3^- + 4h^+ \rightarrow O_2 + 2H_2O + 4CO_2, \quad E^o = +0.765\,V \qquad [7b]$$

The thermodynamic potential required for the production of the various products of Eqs. 5 to 7,

$$U_\theta = E^o_{O_2} - E^o_i, \qquad [8]$$

lies between 1.06 and 1.45 V for the neutral case (mean = 1.23 V), and between 1.23 and 1.33 V for the alkaline case (mean = 1.28 V).

The catalysts considered (silver, copper, platinum, and cobalt oxide) and their reported activity in different electrolytes (NaOH, KOH, and $KHCO_3$), allowed us to define three possible device configurations: *i*) an Ag-Pt system in 1M KOH, *ii*) an Ag-Co system in 1M NaOH, and *iii*) a Cu-Pt system in 0.1M $KHCO_3$. The electrocatalytic parameters necessary for Eqs. 2 and 3, namely i_0, i_{lim}, and α, were extracted from experimental measurement[41,42,24,16,43] by linear least squares fitting. The computed values are presented in Table I.

For copper and platinum catalysts in neutral solution, two overpotential ranges were defined. Separate i_0 and α were computed for all the products except for methane. This approach allowed for a better approximation of the experimentally observed overpotential behavior. The comparison between the experimental data and the fitting parameters of Table I are illustrated in Figures S1-S5.

The parameters in Table I should be interpreted with care as they mainly represent fitting parameters. However, a few observations are noted. Carbon monoxide formation on copper was low at small overpotentials (Tafel slope around −784 mV/dec). At higher overpotentials, the carbon monoxide formation on copper decreased (Tafel slope around +182 mV/dec), because instead, carbon dioxide was used in the formation of other products.[16] Similar observations are made for formate, ethylene, and ethanol, i.e. their formation increases at lower overpotentials and decreases again at higher overpotentials. The evolution of hydrogen and methane increased continuously.

With silver, the hydrogen and carbon monoxide showed similar Tafel slopes while the exchange current densities differed by about an order of magnitude, favoring the formation of CO.

In the alkaline solutions, cobalt oxide was more effective at oxidizing water than platinum. The Tafel slope of cobalt oxide was a factor of two lower than the Tafel slope of platinum, even though its exchange current density was an order of magnitude lower (see Figure S3).

Photoabsorber.—Two sets of PV cells were considered in this study: *i*) currently available cells, and *ii*) cells with optimized performance. Three multi-junction PV cells were considered for the PEC device composed of currently available materials. This choice was based on their open circuit potential, V_{oc}, of the PV component, which had to be larger than the minimal potential required to drive the reactions (U_θ = 1.333 V). The selected PV cells were: *i*) a triple junction cell made of GaInP/GaInAs/Ge, *ii*) a double junction cell made of InGaP/GaAs, and *iii*) a Si-based cell utilizing four cells in series. The experimental performance data was extracted from literature for the three cells.[37–39] The GaInP/GaInAs/Ge cell was utilized due to its high efficiency,[37] keeping in mind that such a cell would be extremely expensive and potentially only able to be implemented when using highly concentrated irradiation.[44] In an attempt to reduce the complexity and cost of the PV cell, a tandem InGaP/GaAs cell was considered,[38] and a PV cell made of four crystalline single-junction Si cells in series was considered in order to use earth abundant and therefore less costly, as well as scalable, components.[39] The open circuit potential, V_{oc}, short current density, i_{sc}, and fill factor (FF) of the three cells considered are summarized in Table II. The expensive triple-junction cell shows the largest V_{oc} and i_{sc}. The earth abundant Si-based PV component shows acceptable V_{oc} at reduced current densities. The Ga-based tandem PV cell shows the lowest V_{oc} of all the PV cells considered.

Additionally, two PV cells were modeled using diode-type equations (see Eq. 1) in order to analyze the influence of the PV performance and its optimization on overall PEC device performance.

Table II. Characteristics of the three realistic PV cells used.

Semiconductor	V_{oc} (V)	i_{sc} (mA/cm^2)	FF (%)
InGaP/GaAs	2.03	11.90	78.9
4-Si	2.45	8.50	77.3
GaInP/GaInAs/Ge	2.57	12.23	86.6

These PV cells were composed of tandem cells utilizing a top layer with a bandgap of 1.8 eV and a bottom layer with a bandgap of 1.2 or 1.4 eV. These bandgap combinations allowed for a sufficiently large V_{oc} in order to drive the reaction. i_{sc} and V_{oc} were calculated using the Shockley-Queisser limit.[40] For each combination, the ideal case with negligible R_s and infinitely large R_{sh} was considered, and then individually, R_s was either increased to around 40 MΩcm^2 or R_{sh} was reduced to 0.6 kΩcm^2. These R_s and R_{sh} were selected in order to compare solar cells with the same fill factor (90, 85, 80, and 75%). The characteristics of the PV cells used for the analysis are shown in Table V.

Electrolyte.—Three different electrolytes were considered according to the reported catalyst characteristics: sodium hydroxide (NaOH), potassium hydroxide (KOH), and potassium bicarbonate ($KHCO_3$). These salts are easy to handle and provide a non-limiting ion conductivity when dissolved in water at a reasonable concentration. At the same time, the catalysts investigated show reasonable stability in theses electrolytes. The ion conductivity of the various electrolytes was 16.45 S/m for 1M NaOH, 19.86 S/m for 1M KOH, and 0.86 S/m for 0.1M $KHCO_3$. The conductivity of the wet Nafion membrane was 10 S/m.

Operational conditions.—Two cases were considered for the solar irradiation conditions: *i*) a 1.5AM spectral distribution at constant irradiation of 1000 W/m^2, and *ii*) a 1.5AM spectral distribution at varying irradiation conditions according to the daily and yearly variation in Barstow, CA, USA. The latter case allowed us to understand and quantify the variation in device performance and product composition with varying irradiation conditions due to daily and yearly variations at a specific location, and to device installation at different locations.

Two scenarios were analyzed for the transient case. One scenario accounted for the irradiation variation during the first five days of January, corresponding to the most difficult condition experienced during the year, since the solar irradiation is low and varies significantly from one day to another. The second case accounted for the first five days of July, corresponding to the most interesting operational conditions, since the solar irradiation has a large magnitude and is more stable during the day. The detailed irradiation magnitudes and variations are shown in Figure S6.

Results

First, we present the performance of the integrated water and CO_2 splitting PEC device using available photoabsorbers and electrocatalysts at steady state. In the second part, we present the performance of the PEC device design simultaneously utilizing a combination of cathodic catalysts. Third, we explore a range of ideal electrocatalysts and photoabsorbers. Finally, we analyze the best PEC design utilizing available components under transient irradiation conditions.

Reference design with available components.—The current density-voltage characteristics of the three PV devices (InGaP/GaInAs/Ge, InGaP/GaAs, and 4-Si) and the three membrane-separated electrocatalysts in their corresponding electrolyte (Ag-Pt in 1M KOH, Ag-Co in 1M NaOH, and Cu-Pt in 0.1M $KHCO_3$) for the sandwich device design (see Figure 2a) and using only one cathode-side catalyst ($n_B = l_B = 0$) are shown in Figure 3. The two silver-based PEC devices showed a weaker increase in potential with increasing current compared to the device in neutral conditions. This was mainly related to the significantly lower conductivity in the electrolyte, resulting in a difference of potential loss in the solution by about an order of magnitude (Figures 4 and 5), and sluggish cathodic reactions, which also produced other products besides CO and hydrogen. The latter were slightly counterbalanced by the relatively efficient oxygen evolution reaction compared to the alkaline systems, where the oxygen evolution reaction required larger overpotentials at a comparable operating current (400 mV in an Ag-Co/InGaP-GaAs device versus

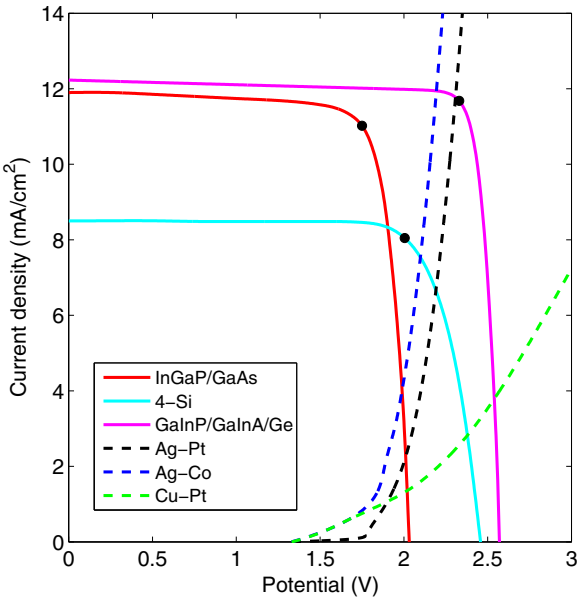

Figure 3. Current density-voltage characteristics of the three realistic PV cells considered (solid lines), and the three membrane-separated electrocatalysts (dashed lines). The operating current density is given by the intersection of the PV and electrolyzer curves. The black dots represent the maximum power point of the PV cells.

238 mV in a Cu-Pt/GaInP-GaInAs-Ge device, both operating near 3.8 mA/cm^2).

The Cu-based device produced a variety of other products not necessarily desirable in our solar fuel processing system, which rather aims at syngas and eventually liquid fuel production. Note that all cathodic reactions work in parallel. Therefore, the sum of the overpotentials does not describe the potential drop at the cathode, instead the potential difference between the electrode and the electrolyte at the interface is constant for all reactions and given by the sum of the overpotential and the equilibrium potential ($\phi_s - \phi_l = \eta_j - E_j^o$ for all cathode reactions described by Eqs. 5 or 6). For all PV components

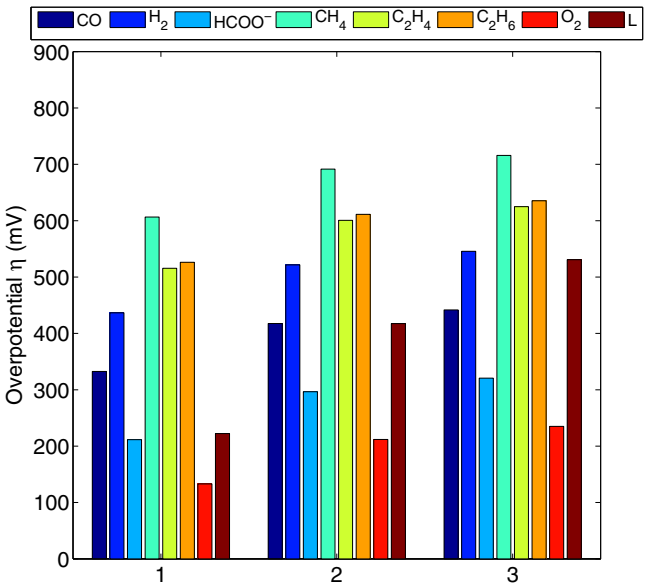

Figure 4. Overpotentials for the generation of each product and ohmic losses in the electrolyte (L) for Cu-Pt catalysts in 0.1M $KHCO_3$. The x-axis indicates the PV cell choice, 1: InGaP/GaAs, 2: 4-Si, 3: GaInP/GaInAs/Ge.

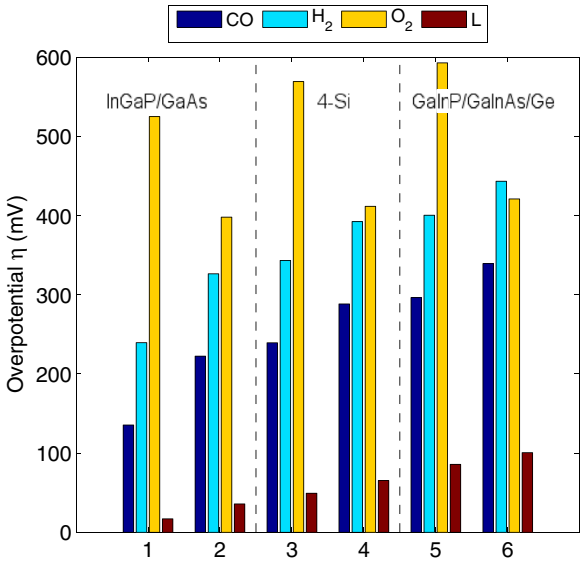

Figure 5. Overpotentials for the generation of each product and ohmic losses in the electrolyte (L) for alkaline PEC devices. The *x*-axis represents the Ag-Pt electrodes (numbers 1, 3, and 5) and the Ag-Co electrodes (numbers 2, 4, and 6).

investigated, in the neutral solution the fraction (in terms of molar flow rates) of produced syngas to all cathodic products was between 62% and 66%, and the fraction of produced CO to all cathodic C-based products was between 21% and 14%. The efficiency, molar product rates, and H_2/CO fractions of the different devices are summarized in Table III. The operational current density for the PEC device using the double-junction solar cell was significantly below the maximum power point (MPP) resulting in η_{PEC} of 3.01% for the Ag-Pt-based device, 5.35% for the Ag-Co-based device, and 1.81% for the Cu-Pt-based device. This combination indicated a non-optimal configuration resulting mainly from the low V_{oc} of this cell. A device using the PV cell composed of four in-series Si-based (4-Si) cells generally improved the efficiency by about a factor of two, i.e. η_{PEC} of 8.88% for the Ag-Pt-based device, 10.04% for the Ag-Co-based device, and 3.76% for the Cu-Pt-based device. This was observed even though the 4-Si cell's i_{sc} was 1.4 times lower than the i_{sc} of the double-junction Ga-based cell. The highest device efficiencies were observed for a device using the triple-junction Ga-based cell, i.e. η_{PEC} of 15.70% for the Ag-Pt-based device, 15.92% for the Ag-Co-based device, and 5.05% for the Cu-Pt-based device.

Because the Ag-Co system was shown to achieve higher efficiencies than the other systems, we used this system in the subsequent analysis.

The H_2/CO ratio was around 0.1 for the Ag-based devices, while it was above 5 for the Cu-based devices. The H_2/CO ratio stayed constant for the Ag-Co-based device when changing the photoabsorbers because of similar Tafel slopes of the hydrogen and CO evolution reactions (see Table I). The ratio increased 2.1 times for the Cu-based device and decreased 1.4 times for the Ag-Pt-based device when changing the photoabsorber from the dual-junction to the triple-junction Ga-based cell.

The systems in alkaline solutions produced more carbon monoxide than hydrogen regardless of the semiconductor used. This agrees with the Tafel slope and the exchange current density analyzed in the electrocatalysts section. The H_2/CO ratio of approximately 0.1 was much smaller than required in our FT reactor. For the system in neutral solution the inverse situation occurred, and more hydrogen was produced than carbon monoxide, i.e. a larger H_2/CO ratio.

Alternative designs.—The production of hydrogen must be increased in the most efficient PEC device (Ag-Co-based) to be usable in the system described in Figure 1, achieving a H_2/CO ratio near 2. The design of the integrated PEC device (sandwich versus side-by-side, Figure 2) and the addition of an extra catalyst, exhibiting a better hydrogen production selectivity at the cathodic side, were considered. Nickel was evaluated as a good option because it's an earth-abundant material and allows for the selective generation of hydrogen.[43] Nickel has a smaller Tafel slope than silver (141 compared to 212.1 mV/dec) at a similar i_0 (8.31e-3 compared to 14e-3 mA/cm^2) resulting in a higher production of hydrogen at a significantly lower overpotential. These alternative designs were investigated using a 4-Si solar cell, a more earth-abundant material choice.

Different versions of silver-nickel arrangements were investigated: a sandwich design (version 1, V1), and a side-by-side design (version 2, V2), as depicted in Figure 2 for $n_A = n_B = 1$ with A = silver and B = nickel. Versions 3 (V3) and version 4 (V4) are analogous to V1 and V2, respectively, with the difference of A = nickel and B = silver. The normalized width of silver is given by the fraction $l_{silver}/(l_{silver}+l_{nickel})$ and was varied for each version of the device design in order to find the least expensive device, i.e. the device requiring the smallest amount of silver to achieve a H_2/CO ratio near 2.

Figure 6 shows the hydrogen and CO production rate normalized by l_{el}, the H_2/CO ratio, and efficiency as function of the silver fraction

Table III. Molar flow rates of CO and H_2, H_2/CO ratio, and efficiency of the PEC devices composed of various combinations of realistic PV cells and membrane-separated electrocatalysts. The device using Cu-based electrodes additionally shows the fraction of CO to all carbon-based products, and the fraction of syngas to all products at the cathode.

		Photoabsorber		
Electrolyzer	Product characteristics	InGaP/GaAs	4-Si	InGaP/GaInAs/Ge
Ag-Pt in 1M KOH	$\dot{n}_{CO}$ (μmol m^{-2} s^{-1})	105.1	316.9	566.1
	$\dot{n}_{H_2}$ (μmol m^{-2} s^{-1})	11.7	28.1	44.1
	H_2/CO (-)	0.112	0.089	0.078
	η_{PEC} (%)	3.01	8.88	15.70
Ag-Co in 1M NaOH	$\dot{n}_{CO}$ (μmol m^{-2} s^{-1})	184.1	344.4	545.4
	$\dot{n}_{H_2}$ (μmol m^{-2} s^{-1})	24	46	73.5
	H_2/CO (-)	0.130	0.134	0.135
	η_{PEC} (%)	5.35	10.04	15.92
Cu-Pt in 0.1M $KHCO_3$	$\dot{n}_{CO}$ (μmol m^{-2} s^{-1})	5.5	6.3	6.1
	$\dot{n}_{H_2}$ (μmol m^{-2} s^{-1})	27.8	47.2	66.4
	H_2/CO (-)	5.062	7.527	10.83
	η_{PEC} (%)	1.81	3.76	5.05
	$\dot{n}_{CO}/\dot{n}_{C-prod}$ (%)	21.4	16.5	13.9
	$(\dot{n}_{CO}+\dot{n}_{H_2})/\dot{n}_{cathode-prod}$ (%)	62.33	62.81	65.81

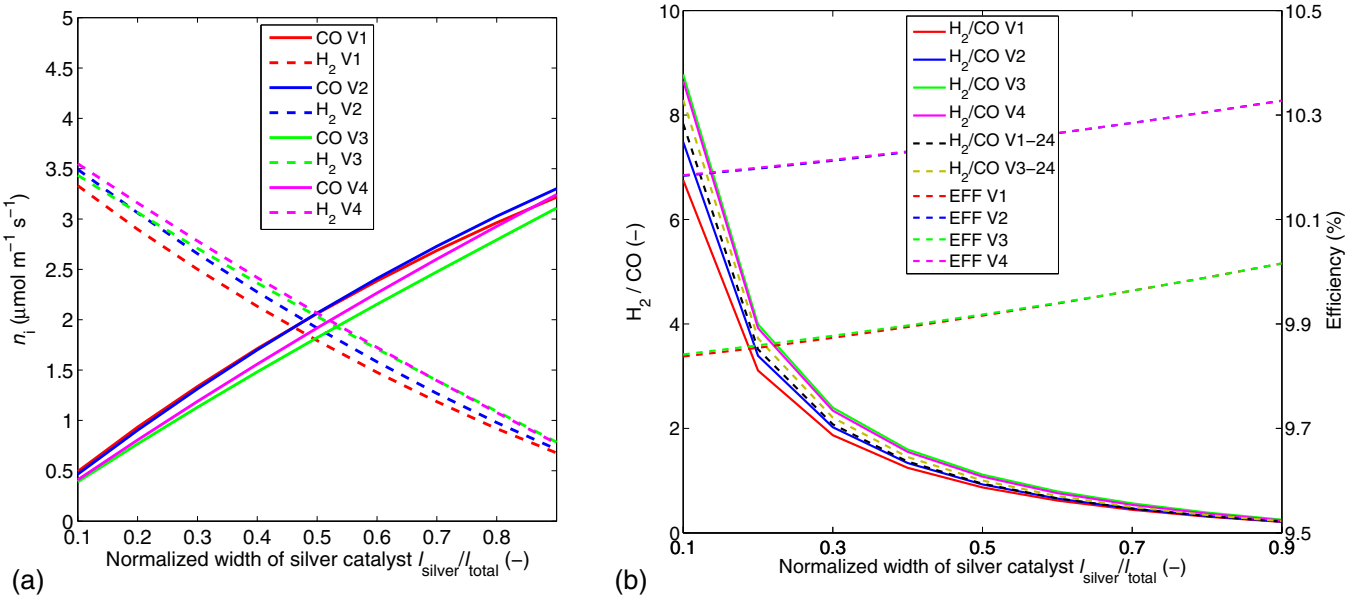

Figure 6. a) CO and H_2 production, b) H_2/CO ratio and efficiency of the PEC device as function of the normalized width of silver for the Ag-Ni/Co systems in an alkaline solution (1M NaOH) connected to a 4-Si solar cell. Version 1 and 3 correspond to the sandwich design of Figure 2a. Version 2 and 4 correspond to the side-by-side design of Figure 2b. All versions have four equally sized patches of silver and nickel per electrode. V1 and V2 have the silver patch closest to the membrane, while V3 and V4 have the nickel patch closest to the membrane. V1-24 and V3-24 indicate the same design as V1 and V3, respectively, but with a larger number of smaller catalyst patches.

of the electrode for the four different design versions. It is apparent that the presence of nickel helps to increase the amount of hydrogen. V3 and V4 produce the largest amount of hydrogen. This is due to the current redistribution in the electrode and the corresponding higher current density close to the membrane (as depicted in Figure S7 and in accordance with Haussener et al.[12]) where the Ni catalyst patch is located. Since a higher current density is available close to the membrane, the nickel catalyst in V3 and V4 uses it only for the generation of hydrogen. In V1 and V2, the silver catalyst is located close to the membrane and uses proportionally more of the higher current density for the generation of carbon monoxide.

V2 and V4 reach higher efficiencies than V1 and V3, consistent with the observations in Haussener et al.[12] and explained by the smaller current densities in V2 and V4 compared to V1 and V3. This is due to the orthogonalization of solar irradiation and the main ion conduction path, allowing for an area expansion and a corresponding decrease in current density, and consequently smaller ohmic losses in the solution.

A larger amount of silver was required for V2, V3, and V4 compared to V1 (Figure 6b and Table IV) to reach a H_2/CO ratio of 2, making them more expensive device choices. This is explained by the smallest observed hydrogen production for device V1 and an associated smaller requirement for the production of CO, resulting in a reduced need for silver.

Adapted V1 and V3 designs (V1-24 and V3-24) were investigated with increased n_A and n_B. These designs attempted to more accurately represent the electrodes, which were prepared by, for example, sputtering techniques with small patch sizes and less predictable patch position. Figure 6b shows the H_2/CO ratio for $n_A = n_B = 6$ and varying l_A and l_B, indicating a requirement for a larger amount of silver in V1-24 to get the same H_2/CO ratio as in the original V1. Hydrogen generation was improved since the width of silver close to the membrane of V1-24 was reduced, allowing the nickel to profit from higher current densities closer to the membrane. The opposite is true for V3-24, where using more patches reduced the amount of required silver compared to the original V3. In this case the hydrogen generation is reduced as the silver electrode is also exposed to higher current densities.

Table IV. Required fraction of the PEC electrode to be made of silver in order for the device to produce hydrogen and CO with a ratio H_2/CO between 1.7-2.15, and the corresponding efficiency of the PEC device.

Version	Normalized silver length (%)	Efficiency (%)
1	32-27	9.88-9.87
2	34-29	10.22-10.21
3	38-32	9.89-9.88
4	37-32	10.23-10.22
1-24	34-29	9.96-9.93
3-24	36-31	9.97-9.94

Photoabsorber and electrocatalyst optimization.—*Ideal catalyst.*—The reporting on cathodic catalysts has illustrated the difficulties in generating H_2/CO ratios in the range required for the generation of synthetic fuels. For this reason, we determine here the electrochemical properties of an ideal catalyst to comply with our requirements.

The influence of the electrochemical properties of the electrodes (i_0 and α) on PEC device performance were analyzed. The exchange currents for hydrogen and CO generation were varied between 1e-5 and 1 and transfer coefficients were varied from 0.1 and 1.

These parameters were selected in an attempt to cover a wide range of possible and desired values (Table I). The electrochemical properties of Ag-Co in a 1 M NaOH electrolyte were used as reference values ($i_{0,CO} = 0.39$ mA/cm^2, $\alpha_{CO} = 0.128$, $i_{lim,CO} = 72.24$ mA/cm^2, $i_{0,H2} = 0.014$ mA/cm^2, $\alpha_{H2} = 0.137$, $i_{lim,H2} = 7.229$ mA/cm^2, $i_{0,O2} = 1.23 \cdot 10^{-7}$ mA/cm^2, and $\alpha_{O2} = 0.726$) and the anode side was kept constant throughout the investigation. The catalysts were integrated with the PV cell utilizing four single-junction silicon cells in series.

Figure 7 shows the achieved H_2/CO ratios with different combinations of exchange current densities of carbon monoxide and hydrogen, with fixed charge transfer coefficients and limit current densities for both products. A range of H_2/CO ratios between $4 \cdot 10^{-5}$ and $1.7 \cdot 10^4$ was observed for the $i_{0,j}$ considered. The smallest H_2/CO ratios were obtained for small $i_{0,H2}$ and large $i_{0,CO}$, while the largest H_2/CO ratios were obtained for large $i_{0,H2}$ and small $i_{0,CO}$. The required H_2/CO ratio for our FT reactor was achieved with a variety of combinations of

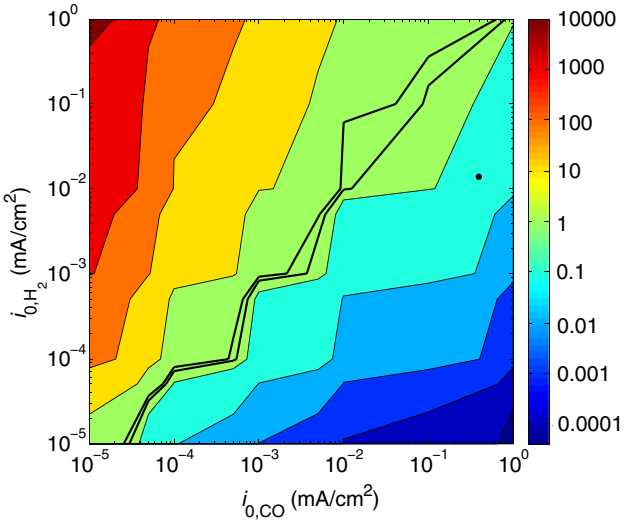

Figure 7. H_2/CO ratio calculated for different combinations of exchange current densities of CO and H_2 with fixed charge transfer coefficients and limiting currents for CO and H_2 ($\alpha_{CO} = 0.128$, $i_{lim,CO} = 72.24$ mA/cm^2, $\alpha_{H_2} = 0.137$, $i_{lim,H_2} = 7.229$ mA/cm^2). The two black lines indicate the range in which the H_2/CO ratio is between 1.7-2.15. The reference case, Ag-Co in 1M NaOH, is indicated by the black dot.

electrochemical properties approximated by the relation $\log_{10}(i_{0,CO}) = 1.1364 \cdot \log_{10}(i_{0,H2}) + 0.2273$ ($i_{0,j}$ in mA/cm^2). From an efficiency point of view, not all of these combinations are as desirable. Figure S8 shows the same combinations of $i_{0,H2}$ and $i_{0,CO}$ and their corresponding efficiency, indicating that combinations leading to a H_2/CO ratio of around 2 have the potential to exhibit efficiencies anywhere from 1% to 10%. Combinations with large $i_{0,j}$ are required to achieve high efficiencies.

Figure 8 shows the calculated H_2/CO ratios with different combinations of exchange current density and transfer coefficient of CO with fixed hydrogen kinetics. The variations in α_{CO} and $i_{0,CO}$ considered resulted in an achievable H_2/CO ratio between $7.2 \cdot 10^{-3}$ and $7.1 \cdot 10^{3}$. The silver electrode used as a reference case could attain the required H_2/CO ratio only if it was modified (its $i_{0,CO}$ decreased to around $3 \cdot 10^{-2}$ mA/cm^2). A smaller number of combinations could achieve the required H_2/CO ratio for our FT reactors compared to the previous case and is approximated by the relation $\alpha_{CO} = -0.0641 \cdot \log_{10}(i_{0,CO}) + 0.0297$ ($i_{0,CO}$ in mA/cm^2). The efficiency for these combinations stays constant at around 7.5% (Figure S9).

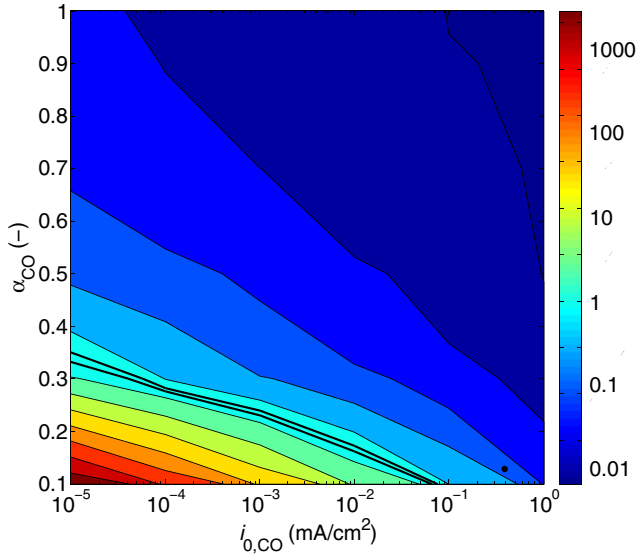

Figure 8. H_2/CO ratio calculated for different combinations of exchange current densities and charge transfer coefficients of CO with fixed properties for H_2 generation ($i_{0,H_2} = 0.014$ mA/cm^2, $\alpha_{H_2} = 0.137$, $i_{lim,H_2} = 7.229$ mA/cm^2). The two black lines indicate the range in which the H_2/CO ratio is between 1.7-2.15. The reference case, Ag-Co in 1M NaOH, is indicated by the black dot.

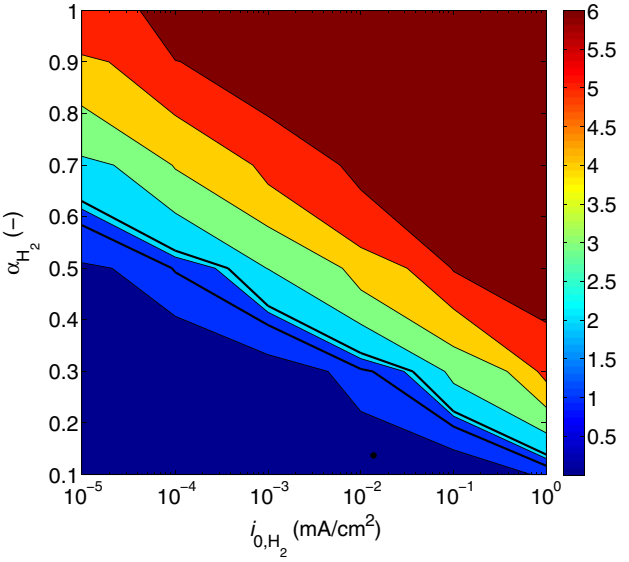

Figure 9. H_2/CO ratio calculated for different combinations of exchange current densities and charge transfer coefficients of H_2 with fixed properties for CO generation ($i_{0,CO} = 0.39$ mA/cm^2, $\alpha_{CO} = 0.128$, $i_{lim,CO} = 72.24$ mA/cm^2). The two black lines indicate the range in which the H_2/CO ratio is between 1.7-2.15. The reference case, Ag-Co in 1M NaOH, is indicated by the black dot.

Figure 9 shows the calculated H_2/CO ratios with different combinations of exchange current density and charge transfer coefficient of hydrogen with fixed electrochemical properties for the CO kinetics. The calculated H_2/CO ratio ranged between $3.3 \cdot 10^{-5}$ and 6.7 for the considered range in α_{H2} and $i_{0,H2}$, a smaller range compared to that available when varying the CO kinetics. Nevertheless, there is a larger number of possible combinations to achieve H_2/CO ratios of around 2 compared to the previous case. These combinations are approximated by the relation $\alpha_{H2} = -0.0920 \cdot \log_{10}(i_{0,H2}) + 0.14$ ($i_{0,H2}$ in mA/cm^2). The efficiency for all the combinations which reach the required H_2/CO ratio is approximately 10.6% (Figure S10).

Ideal photoabsorber.—The performance of the Ag-Co system in alkaline solution (1M NaOH) and Cu-Pt system in neutral solution (0.1M $KHCO_3$) with solar irradiation at standard conditions were analyzed for a variety of combinations of solar absorbers. The tandem absorber was approximated by Eq. 1. Two sets of representative tandem cells were chosenusing top and bottom cells with band gaps of: *i*) 1.8 and 1.2 eV, and *ii*) 1.8 and 1.4 eV. For PEC cells made of any combination of the two tandem cells and of the two electrolyzers (Ag-Co and Cu-Pt), a significant improvement in efficiency was achieved when the series resistance was small and the shunt resistance was large, Table V. The impact of the series resistance on efficiency was larger for cells operating at voltages close to the MPP. The series resistance had no influence on the performance for cells with large V_{oc} and those operating at voltages much smaller than the voltage of the MPP, i.e. in the plateau region of the *iV*-curve. The shunt resistance had a larger impact on the performance of the cells operating at voltages below or around the voltage of the MPP. The shunt resistance had no influence on tandem cells operating above the voltage of the MPP in the steep decrease of the *iV*-curve. Therefore, no change in η_{PEC} was observed for both of the tandem cells operating in the neutral solution.

Table V. H_2/CO ratio and efficiency of the two sets of tandem cells with band gaps of 1.8 and 1.2 eV (i_{sc} = 19.6 mA/cm^2) or 1.8 and 1.4 eV (i_{sc} = 13.2 mA/cm^2) using the Ag-Co alkaline electrolyzer or the Cu-Pt neutral electrolyzer for varying R_s and R_{sh}. Solar irradiation was 1000 W/m^2 at the 1.5AM spectrum and 300 K.

i_{sc} (mA/cm^2)	V_{oc} (V)	R_s (MΩ cm^2)	R_{sh} (kΩ cm^2)	FF (%)	H_2/CO (-)	η_{PEC} (%)
using Ag-Co alkaline electrolyzer						
19.6	2.31	3, 11, 17, 23	10000	90, 85, 80, 75	0.1346, 0.1347, 0.1344, 0.1339	19.60, 14.57, 12.41, 10.85
13.2	2.50	2, 19, 28, 38	10000	93, 85, 80, 75	0.1347, 0.1348, 0.1346, 0.1342	17.59, 16.40, 13.88, 11.86
19.6	2.31	3	10000, 1.40, 0.82, 0.58	90, 85, 80, 75	0.1346, 0.1346, 0.1346, 0.1347	19.60, 19.20, 18.84, 18.37
13.2	2.50	2	10000, 1.92, 1.22, 0.89	93, 85, 80, 75	0.1347, 0.1347, 0.1347, 0.1346	17.59, 16.05, 15.17, 14.31
using Cu-Pt neutral electrolyzer						
19.6	2.31	3, 11, 17, 23	10000	90, 85, 80, 75	6.63, 6.46, 6.35, 6.25	3.26, 3.15, 3.07, 2.99
13.2	2.50	2, 19, 28, 38	10000	93, 85, 80, 75	9.44, 8.44, 7.99, 7.61	4.57, 4.18, 3.98, 3.80
19.6	2.31	3	10000, 1.40, 0.82, 0.58	90, 85, 80, 75	6.63, 6.63, 6.62, 6.62	3.26, 3.26, 3.26, 3.26
13.2	2.50	2	10000, 1.92, 1.22, 0.89	93, 85, 80, 75	9.44, 9.43, 9.42, 9.41	4.57, 4.57, 4.56, 4.56

The series and shunt resistances had no influence on the H_2/CO ratio of the cells operating in alkaline solution (Ag-Co system). This was explained by the similar Tafel slope of the CO and H_2 generation reactions (Table I) and the small change in operating current.

For the copper case, there was a more interesting change in the H_2/CO ratio when the series resistance was decreased, but the results were still far from the desired ratio.

Operational conditions.—The generated hourly ratio of H_2/CO during the first five days of January and July using the V1 design and Ag-Ni/Co electrodes with 27% silver catalysts, and an ideal tandem cell with band gaps of 1.8 eV and 1.2 eV (R_s = 3 MΩcm^2, R_{sh} = 10 MΩcm^2), is shown in Figure 10. Variations in the ratio followed the variations of daily solar irradiation with maximum values at noon. It was possible to achieve the required H_2/CO ratios for our FT reactors in January and July, but they were limited to specific hours of the day, requiring the addition of a water gas shift reactor or the local storage of the products before their use in order to counter balance the low H_2/CO ratios before and after noon and the high H_2/CO at noon. Figure 11 shows the cumulative daily production of hydrogen and CO, and the related H_2/CO ratio for the first five days of January and July. In both cases, the ratio of the products reached a maximum and then decreased reaching a constant value. This decrease was observed at the end of the day where the solar irradiation, and consequently the operating current, was low, favoring the production of carbon monoxide. An average daily H_2/CO ratio of 1.82 was reached at the end of the day in January, which was within the requirements for our FT reactor using an iron-based catalyst.

In the July case, an average daily H_2/CO ratio of 2.46 was reached at the end of the day, which was slightly above the required ratio for our FT reactor. A slight excess of hydrogen was produced in July and a slight excess of CO was produced in January. Four possibilities for alleviating the slight mismatch of the H_2/CO ratio could be considered: seasonal product storage, hydrogen separation and storage during high-irradiation seasons for use in seasons where the product is scarce, the addition of a water gas shift reactor, or the use of two types of FT reactors adapted to the product ratio of cold and warm seasons.

Conclusions

We developed a modeling framework for the investigation of the performance of a photoelectrochemical (PEC) device allowing for the concurrent splitting of water and CO_2 into hydrogen and CO, i.e. synthesis gas. The synthesis gas is capable of being further processed into liquid fuels via large-scale commercial Fischer-Tropsch plants. This pathway is consistent with a second artificial solar fuels pathway, the

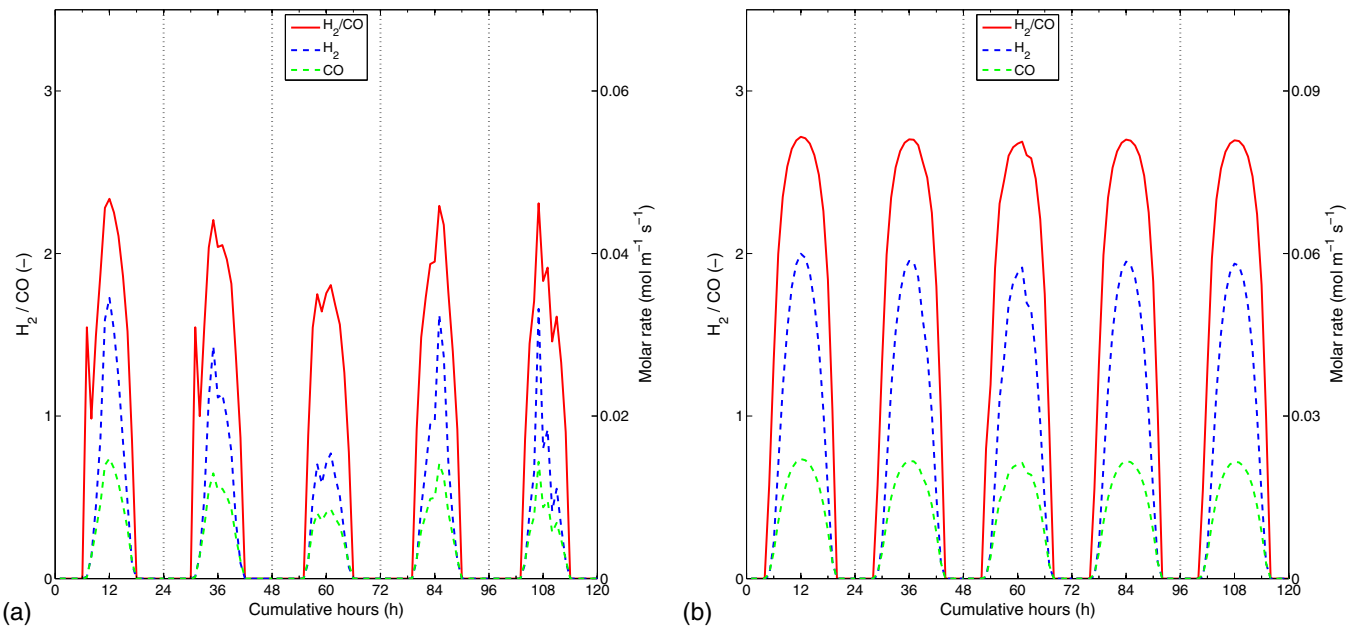

Figure 10. Instantaneous H_2/CO ratio (solid line, left y-axis) and molar production rates of CO and H_2 (dashed lines, right y-axis) generated by a Ag-Ni/Co system in alkaline solution during the first five days of (a) January, and (b) July, in Barstow.

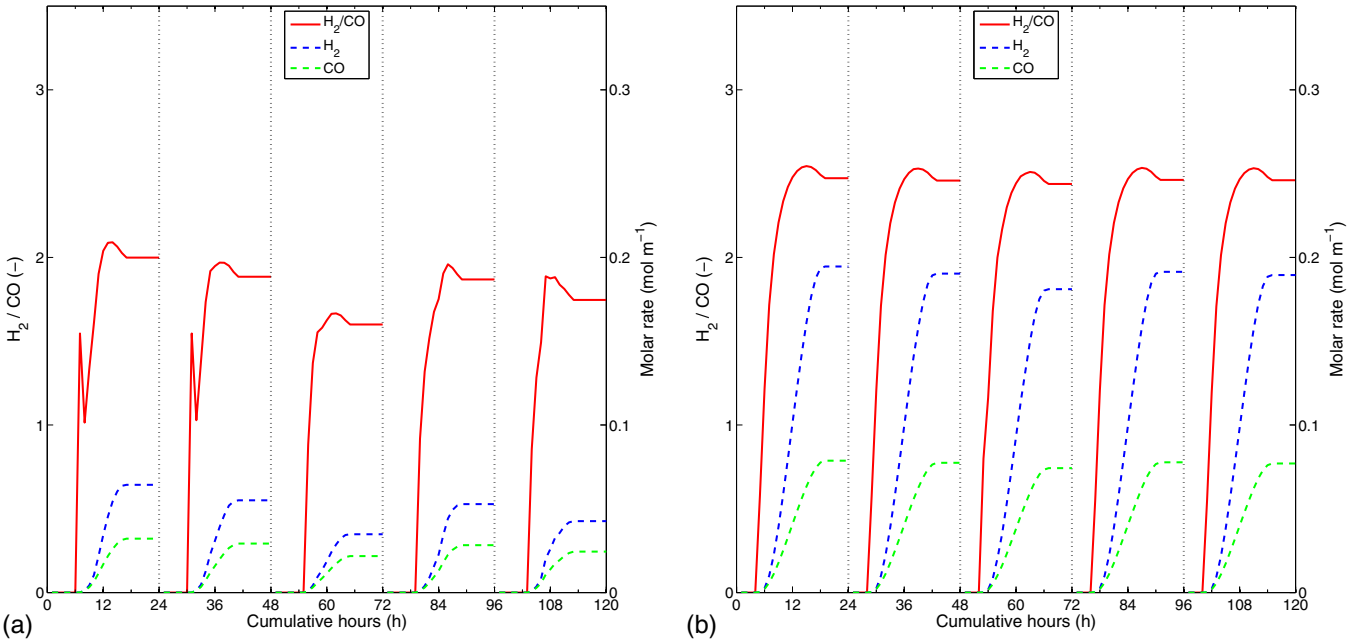

Figure 11. Daily cumulative H_2/CO ratio (solid line, left y-axis) and molar production rates of CO and H_2 (dashed lines, right y-axis) generated by a Ag-Ni/Co system in alkaline solution during the first five days of (a) January, and (b) July, in Barstow.

solar thermochemical production of synthesis gas, and consequently provides a consistent approach to a future solar fuel economy, as both approaches would utilize the same post-processing and distribution infrastructure.

Two types of realistic PEC devices were evaluated utilizing two different electrolytes, an alkaline solution and a pH-neutral solution, with corresponding electrocatalyst combinations (Ag-Pt and Ag-Co, or Cu-Pt). In both systems, solar irradiation was used as the source of energy and transformed into electrical energy using three types of catalyst-coated photovoltaic (PV) cells with varying combinations of open circuit potentials, short current densities, and fill factors.

The results showed that for Ag-based electrodes the selection of the PV did not significantly affect the H_2/CO ratio, because the generation rate of carbon monoxide and hydrogen increased at a similar rate with increasing potential. On the other hand, when using a Cu-based electrode, the PV cell selection was important, because the H_2/CO ratio changed significantly due to a reduced production of carbon monoxide at large potentials. Copper was able to achieve the desired H_2/CO ratio of 2 (interesting for the Fischer-Tropsch based production of liquid fuels) using solar cells with smaller V_{oc}. However, the produced syngas rate was too small for the device to be competitive, owing to the small operating current densities as well as to the production of other products (in the range of 35–40%) not considered relevant in our system. Of the three analyzed catalyst-electrolyte systems, the Ag-Co-based system required the smallest overpotentials, and therefore exhibited the largest operational current densities in combination with any of the PV cells.

Owing to the low H_2/CO product ratio in the Ag-Co-based system, we added nickel to the cathode in order to increase the amount of hydrogen. We demonstrated that the position and the width of the nickel electrode affects the performance of the PEC device, generating higher amounts of hydrogen when nickel is applied on electrode locations closer to the membrane. Consequently, a tailored application of the two catalysts (less costly Ni and expensive Ag) on the cathode provide inexpensive PEC devices with the same product composition.

A parametric study of the catalyst characteristics was conducted in order to provide design guidelines for novel catalysts for enhanced PEC device efficiency and product selectivity. For a PEC device utilizing 4-Si PV cells, while keeping all other catalytic properties at the Ag-Co reference case, an H_2/CO ratio of 2 is achieved when the exchange current densities of the CO_2 reduction and hydrogen evolution reaction catalysts are related by the relation $\log_{10}(i_{0,CO}) = 1.1364 \cdot \log_{10}(i_{0,H2}) + 0.2273$ ($i_{0,j}$ in mA/cm^2), providing PEC device efficiencies anywhere from 1 to 10%. Combinations with large exchange current densities favor higher efficiencies. The relation between the transfer coefficient and the exchange current density of the CO_2 reduction catalyst required for a H_2/CO ratio of 2 is $\alpha_{CO} = -0.0641 \cdot \log_{10}(i_{0,CO}) + 0.0297$ ($i_{0,CO}$ in mA/cm^2). All operate at a 7.5% PEC device efficiency.

Ideal PV cells were investigated in order to provide guidelines for the quality requirement of the PV (mostly its FF). Neither the series nor the shunt resistance of the PV significantly affect the product composition of the Ag-Co catalyst in an alkaline electrolyte. These systems suffer from a 10 times larger production of carbon monoxide than hydrogen for a wide range of voltage applied. The influence of series resistance on device performance was more important for a system using copper electrodes, as they generally operate very close to the V_{oc}, i.e. in the falling region of the PV's iV-curve, which is little affected by changes in shunt resistance, but more significantly by changes in series resistance. However, the H_2/CO product ratio remained in the range of 6–10, far from the desired value of 2.

Solar irradiation data measured in Barstow, California, allowed us to perform a time-dependent analysis of an Ag/Ni-Co system with 27%-73% Ag/Ni content. The results revealed that at lower solar irradiation (e.g. at the beginning and end of each day, or during winter), carbon monoxide production is favored, and therefore the H_2/CO ratio decreases, while at higher solar irradiation (e.g. mid-day or in summer), the H_2/CO ratio increases. Consequently, product composition is expected to vary during the day and year, which could be counteracted by adding a water gas shift reactor to the system or local gas storage solutions, eventually providing a more constant product composition to the Fischer-Tropsch plant. Alternatively, the time-dependent composition of the stored products reveals that in cold seasons the stored products could be used in a FT reactor which uses iron-based catalysts (i.e. works well with H_2/CO ratios slightly below 2), while in warmer seasons the products could be used in a FT reactor using cobalt-based catalysts (i.e. works well with H_2/CO ratios slightly above 2).

In conclusion, this study provides insight into the complex operational behavior of an integrated PEC device concurrently producing

hydrogen and carbon monoxide. The framework is a useful tool for formulating quantitative design guidelines for reactor designs, the combination of components and their desired characteristics, and operational conditions. We provide guidance at the materials level for the dedicated design of catalysts and photoabsorbers to be incorporated into an optimized PEC device with desired product composition.

Acknowledgment

This material is based upon work performed with the financial support of The Starting grant of the Swiss National Science Foundation, as part of the SCOUTS project (grant #155876). We thank Dr. Simone Pokrant for fruitful discussions.

References

1. G. P. Smestad and A. Steinfeld, "Review: Photochemical and thermochemical production of solar fuels from h2o and co2 using metal oxide catalysts," *Industrial & Engineering Chemistry Research*, **51**(37), 11828 (2012).
2. M. Romero and A. Steinfeld, "Concentrating solar thermal power and thermochemical fuels," *Energy Environ. Sci.*, **5**, 9234 (2012).
3. W. Lipinski, J. Davidson, S. Haussener, J. Klausner, A. Mehdizadeh, J. Petrasch, A. Steinfeld, and L. Venstrom, "Review of heat transfer research for solar thermochemical applications," *Journal of Thermal Science and Engineering Applications*, **5**, 021005 (2013).
4. J. Ronge, T. Bosserez, D. Martel, C. Nervi, L. Boarino, F. Taulelle, G. Decher, S. Bordiga, and J. A. Martens, "Monolithic cells for solar fuels," *Chem. Soc. Rev.*, **43**, 7963 (2014).
5. P. Furler, J. R. Scheffe, and A. Steinfeld, "Syngas production by simultaneous splitting of h2o and co2 via ceria redox reactions in a high-temperature solar reactor," *Energy Environ. Sci.*, **5**, 6098 (2012).
6. J. W. Ager, M. R. Shaner, K. A. Walczak, I. D. Sharp, and S. Ardo, "Experimental demonstrations of spontaneous, solar-driven photoelectrochemical water splitting," *Energy Environ. Sci.*, **8**, 2811 (2015).
7. E. E. Barton, D. M. Rampulla, and A. B. Bocarsly, "Selective Solar-Driven reduction of CO2 to methanol using a catalyzed p-GaP based Photoelectrochemical cell," *Journal of the American Chemical Society*, **130**, 6342 (2008).
8. J. L. White, M. F. Baruch, J. E. Pander III, Y. Hu, I. C. Fortmeyer, J. E. Park, T. Zhang, K. Liao, J. Gu, Y. Yan, T. W. Shaw, E. Abelev, and A. B. Bocarsly, "Light-driven heterogeneous reduction of carbon dioxide: Photocatalysts and photoelectrodes," *Chemical Reviews*, **115**(23), 12888 (2015).
9. M. Schreier, L. Curvat, F. Giordano, L. Steier, A. Abate, S. M. Zakeeruddin, J. Luo, M. T. Mayer, and M. Grätzel, "Efficient photosynthesis of carbon monoxide from co2 using perovskite photovoltaics," *Nature Communications*, **6**, 7326 (2015).
10. M. Schreier, J. Luo, P. Gao, T. Moehl, M. T. Mayer, and M. Grätzel, "Covalent immobilization of a molecular catalyst on cu2o photocathodes for co2 reduction," *Journal of the American Chemical Society*, **138**(6), 1938 (2016).
11. J. Durst, A. Rudnev, A. Dutta, Y. Fu, J. Herranz, V. Kaliginedi, A. Kuzume, A. A. Permyakova, Y. Paratcha, P. Broekmann, and T. J. Schmidt, "Electrochemical co2 reduction a critical view on fundamentals, materials and applications," *CHIMIA International Journal for Chemistry*, **69**(12), 769 (2015).
12. S. Haussener, C. Xiang, J. M. Spurgeon, S. Ardo, N. S. Lewis, and A. Z. Weber, "Modeling, simulation, and design criteria for photoelectrochemical water-splitting systems," *Energy Environ. Sci.*, **5**, 9922 (2012).
13. S. Haussener, S. Hu, C. Xiang, A. Z. Weber, and N. S. Lewis, "Simulations of the irradiation and temperature dependence of the efficiency of tandem photoelectrochemical water-splitting systems," *Energy Environ. Sci.*, **6**, 3605 (2013).
14. Y. Hori, "Co2-reduction, catalyzed by metal electrodes," in *Handbook of Fuel Cells: Fundamentals, Technology and Application*, vol. **2**: 720, A. L. Wolf Vielstich and Hubert A. Gasteiger, Chichester, VHC-Wiley, 2003.
15. G. B. Haxel, J. B. Hedrick, and G. J. Orris, "Rare earth elements—critical resources for high technology." http://pubs.usgs.gov/fs/2002/f s087, 2002. U.S. Geological Survey, Fact Sheet 087.
16. K. P. Kuhl, E. R. Cave, D. N. Abram, and T. F. Jaramillo, "New insights into Electrochemical reduction of carbon dioxide on metallic copper surfaces," *Energy Environ. Sci.*,**5**, 7050 (2012).
17. M. Le, M. Ren, Z. Zhang, P. T. Sprunger, R. L. Kurtz, and J. C. Flake, "Electrochemical reduction of CO2 to CH3OH at copper oxide surfaces," *Journal of The Electrochemical Society*, **158**(5), E45 (2011).
18. C. W. Li and M. W. Kanan, "Co2 reduction at low overpotential on cu electrodes resulting from the reduction of thick cu2o films," *Journal of the American Chemical Society*, **134**(17), 7231, (2012). PMID: 22506621.
19. A. Loiudice, P. Lobaccaro, E. A. Kamali, T. Thao, B. H. Huang, J. W. Ager, and R. Buonsanti, "Tailoring copper nanocrystals toward c2 products in electrochemical co2 reduction," *Angewandte Chemie International Edition*, **55**(19), 5789 (2016).
20. C. Delacourt, *Electrochemical reduction of carbon dioxide and water to syngas (CO + H2) at room temperature*. PhD thesis, University of California Berkeley, 2006.
21. Q. Lu, J. Rosen, Y. Zhou, G. S. Hutchings, Y. C. Kimmel, J. G. Chen, and F. Jiao, "A selective and efficient electrocatalyst for carbon dioxide reduction," *Nature Communications* (2014).
22. Y. Hori, H. Ito, K. Okano, K. Nagasu, and S. Sato, "Silver-coated ion exchange membrane electrode applied to electrochemical reduction of carbon dioxide," *Electrochimica Acta*, **48**, 2651 (2003).
23. T. Hatsukade, K. P. Kuhl, E. R. Cave, D. N. Abram, and T. F. Jaramillo, "Insights into the electrochemical reduction of CO_2 on metallic silver surfaces," *Phys. Chem. Chem Phys.*, **16**, 13814 (2014).
24. M. R. Thorson, K. I. Siil, and P. J. A. Kenis, "Effect of Cations on the Electrochemical Conversion of CO_2 to CO," *Journal of The Electrochemical Society*, **160**(1), F69 (2013).
25. S. Ma, Y. Lan, G. M. J. Perez, S. Moniri, and P. J. A. Kenis, "Silver Supported on Titania as an Active Catalyst for Electrochemical Carbon Dioxide Reduction," *ChemSusChem*, **7**, 866 (2014).
26. C. E. Tornow, M. R. Thorson, S. Ma, A. A. Gewirth, and P. J. A. Kenis, "Nitrogen-Based Catalyst for the Electrochemical Reduction of CO_2 to CO," *Journal of the American Chemical Society*, **134**, 19520 (2012).
27. M. G. Walter, E. L. Warren, J. R. McKone, S. W. Boettcher, Q. Mi, E. A. Santori, and N. S. Lewis, "Solar Water Splitting Cells," *Chemical Reviews*, **110**, 6446 (2010).
28. M. E. Dry, "High quality diesel via the fischer-tropsch process - a review," *Journal of Chemical Technology and Biotechnology*, **77**, 43 (2001).
29. M. D. S. Tembhurne and S. Haussener, "Heat transfer modeling in integrated photoelectrochemical hydrogen generators using concentrated irradiation," in *Proceedings of the 15th International Heat Transfer Conference*, Kyoto, 10 August, 2014.
30. S. Tembhurne and S. Haussener, "Integrated photo-electrochemical solar fuel generators under concentrated irradiation. I. 2-D non-isothermal multiphysics modeling," *Journal of The Electrochemical Society*, **163**(10), H988 (2016).
31. S. Tembhurne and S. Haussener, "Integrated photo-electrochemical solar fuel generators under concentrated irradiation. II. Thermal management a crucial design consideration," *Journal of The Electrochemical Society*, **163**(10), H999 (2016).
32. H. Doscher, J. F. Geisz, T. G. Deutsch, and J. A. Turner, "Sunlight absorption in water - efficiency and design implications for photoelectrochemical devices," *Energy Environ. Sci.*, **7**, 2951 (2014).
33. E. A. Hernandez-Pagan, N. M. Vargas-Barbosa, T. Wang, Y. Zhao, E. S. Smotkin, and T. E. Mallouk, "Resistance and polarization losses in aqueous buffer-membrane electrolytes for water-splitting photoelectrochemical cells," *Energy Environ. Sci.*, **5**, 7582 (2012).
34. M. A. Modestino, K. A. Walczak, A. Berger, C. M. Evans, S. Haussener, C. Koval, J. S. Newman, J. W. Ager, and R. A. Segalman, "Robust production of purified h2 in a stable, self-regulating, and continuously operating solar fuel generator," *Energy Environ. Sci.*, **7**, 297 (2014).
35. J. Newman and K. Thomas-Alyea, *Electrochemical systems*. John Wiley & Sons, 2004.
36. A. Berger, R. A. Segalman, and J. Newman, "Material requirements for membrane separators in a water-splitting photoelectrochemical cell," *Energy Environ. Sci.*, **7**, 1468 (2014).
37. R. R. King, M. Haddad, T. Isshiki, P. Colter, J. Ermer, H. Yoon, D. E. Joslin, and N. H. Karam, "Methamorphic GaInP/GaInAs/Ge Solar Cells," in *28th IEEE Photovoltaic Specialists Conference*, (2000).
38. H. W. Yu, H. Q. Nguyen, C. C. Chung, B. T. Tran, and E. Y. Chang, "InGaP/GaAs Dual-junction Solar cells with Different Tunnel Diodes," *International Journal of Research in Engineering and Technology*, **1**(4), 2277 (2012).
39. C. R. Cox, J. Z. Lee, D. G. Nocera, and T. Buonassisi, "Ten-percent solar-to-fuel conversion with nonprecious materials," *PNAS*, **11**(39), 14057 (2014).
40. W. Shockley and H. J. Queisser, "Detailed balance limit of efficiency of p-n junction solar cells," *Journal of Applied Physics*, **32**(3), 510 (1961).
41. C. Iwakura, K. Fukuda, and H. Tamura, "The anodic evolution of oxygen on platinium oxide electrode in alkaline solutions," *Electrochimica Acta*, **21**, 501 (1976).
42. C. Iwakura, A. Honji, and H. Tamura, "The anodic evolution of oxygen on Co_3O_4 film eelectrode in alkaline solutions," *Electrochimica Acta*, **26**(9), 1319 (1981).
43. N. Krstajic, M. Popovic, B. Grgur, M. Vojnovic, and D. Sepa, "On the kinetics of the hydrogen evolution reaction on nickel in alkaline solution, Part I. The mechanism," *Journal of Electroanalytical Chemistry*, **512**, 16 (2001).
44. M. Dumortier, S. Tembhurne, and S. Haussener, "Holistic design guidelines for solar hydrogen production by photo-electrochemical routes," vol. DOI: 10.1039/C5EE01821H, 2015.